AGU PUBLICATIONS

JGR

Journal of Geophysical Research: Oceans

RESEARCH ARTICLE

10.1002/2014JC009985

Key Point:
- Contemporary snow depth distribution on Arctic sea ice

Supporting Information:
- Readme
- Supplementary Table S1

Correspondence to:
M. A. Webster,
melindaw@uw.edu

Citation:
Webster, M. A., I. G. Rigor, S. V. Nghiem, N. T. Kurtz, S. L. Farrell, D. K. Perovich, and M. Sturm (2014), Interdecadal changes in snow depth on Arctic sea ice, *J. Geophys. Res. Oceans*, *119*, 5395–5406, doi:10.1002/2014JC009985.

Received 20 MAR 2014
Accepted 29 JUL 2014
Accepted article online 2 AUG 2014
Published online 22 AUG 2014

Interdecadal changes in snow depth on Arctic sea ice

Melinda A. Webster[1], Ignatius G. Rigor[1], Son V. Nghiem[2], Nathan T. Kurtz[3], Sinead L. Farrell[3,4], Donald K. Perovich[5], and Matthew Sturm[6]

[1]Polar Science Center, Applied Physics Laboratory, University of Washington, Seattle, Washington, USA, [2]Jet Propulsion Laboratory, California Institute of Technology, Pasadena, California, USA, [3]Hydrospheric and Biospheric Sciences Laboratory, NASA Goddard Space Flight Center, Greenbelt, Maryland, USA, [4]Earth System Science Interdisciplinary Center, University of Maryland, College Park, Maryland, USA, [5]US Army Corps of Engineers, Engineer Research and Development Center, Cold Regions Research and Engineering Laboratory, Hanover, New Hampshire, USA, [6]Geophysical Institute, University of Alaska Fairbanks, Fairbanks, Alaska, USA

Abstract Snow plays a key role in the growth and decay of Arctic sea ice. In winter, it insulates sea ice from cold air temperatures, slowing sea ice growth. From spring to summer, the albedo of snow determines how much insolation is absorbed by the sea ice and underlying ocean, impacting ice melt processes. Knowledge of the contemporary snow depth distribution is essential for estimating sea ice thickness and volume, and for understanding and modeling sea ice thermodynamics in the changing Arctic. This study assesses spring snow depth distribution on Arctic sea ice using airborne radar observations from Operation IceBridge for 2009–2013. Data were validated using coordinated in situ measurements taken in March 2012 during the Bromine, Ozone, and Mercury Experiment (BROMEX) field campaign. We find a correlation of 0.59 and root-mean-square error of 5.8 cm between the airborne and in situ data. Using this relationship and IceBridge snow thickness products, we compared the recent results with data from the 1937, 1954–1991 Soviet drifting ice stations. The comparison shows thinning of the snowpack, from 35.1 $\pm$ 9.4 to 22.2 $\pm$ 1.9 cm in the western Arctic, and from 32.8 $\pm$ 9.4 to 14.5 $\pm$ 1.9 cm in the Beaufort and Chukchi seas. These changes suggest a snow depth decline of 37 $\pm$ 29% in the western Arctic and 56 $\pm$ 33% in the Beaufort and Chukchi seas. Thinning is negatively correlated with the delayed onset of sea ice freezeup during autumn.

1. Introduction

The Arctic is undergoing unprecedented change [*Overpeck et al*., 2005; *National Academies*, 2012]. The trend in sea ice extent is decreasing at an accelerated rate [*Stroeve et al*., 2012], and there has been a shift from thick, multiyear ice to a thinner, younger sea ice regime [*Nghiem et al*., 2007; *Kwok and Rothrock*, 2009; *Maslanik et al*., 2011]. This shift has profoundly affected the state of Arctic sea ice, which has become more dynamic and susceptible to melt, changing the ice volume [*Laxon et al*., 2013], ocean heat flux [*Perovich et al*., 2007], surface albedo [*Perovich and Polashenski*, 2012], and snow cover [*Hezel et al*., 2012].

Snow on sea ice plays a key role in sea ice thermodynamics [*Maykut and Untersteiner*, 1971; *Maykut*, 1986; *Blazey et al*., 2013]. Depending on snow thickness, distribution, and density, it can help recover the sea ice pack, or exacerbate its loss. During the spring, snow thickness limits how much transmittance and absorption of solar energy can occur within the sea ice and underlying ocean [*Perovich and Polashenski*, 2012]. Thick snow may withstand melt and maintain a high surface albedo throughout the summer melt period [*Eicken et al*., 2004]. Conversely, meltwater from thin snow may enhance the formation of melt ponds [*Eicken et al*., 2004; *Petrich et al*., 2012], which absorb 1.7 times more solar radiation than bare sea ice and 5 times more than cold, snow-covered sea ice [*Perovich and Polashenski*, 2012; *Perovich et al*., 2002]. Earlier onset of Arctic sea ice melt has been documented [*Markus et al*., 2009], and likely contributes to earlier spring phytoplankton blooms and shifts in sympagic-based ecosystems [*Arrigo et al*., 2008; *Wassmann et al*., 2011; *Grebmeier et al*., 2010]. In extremely thin snow cases, little meltwater is produced and melt pond formation can be inhibited [*Eicken et al*., 2004].

While a decreasing trend has been reported in most terrestrial regions [*IPCC*, 2013], interdecadal changes of snow depth on Arctic sea ice have not been adequately addressed. A past climatology of snow on Arctic sea ice was developed in the study by *Warren et al*. [1999, hereafter referred to as W99], which used

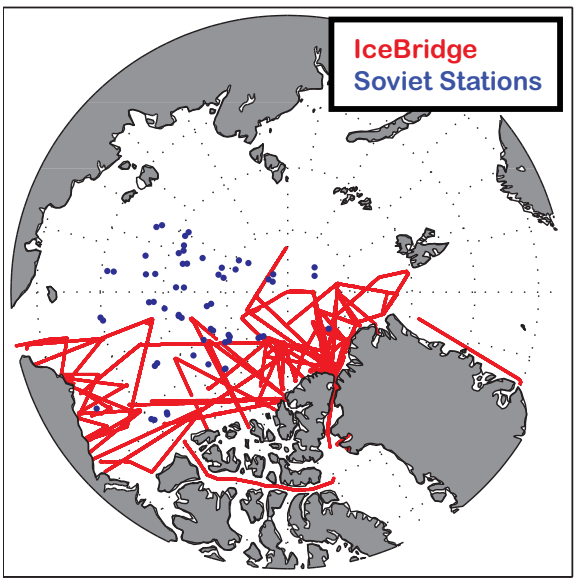

Figure 1. Locations of the 2009–2013 Operation IceBridge flights measuring snow depth (red lines) and 1937, 1954–1991 Soviet station (blue dots) during March and April.

extensive field data from the Soviet drifting ice stations in 1937 and 1954–1991. W99 spring snow depths ranged from a few centimeters on young sea ice to over 40 cm on multiyear sea ice. These values may not be representative of the current conditions of the snow cover [*Kurtz and Farrell*, 2011], and likely contribute to uncertainties in current sea ice thickness and volume estimates [*Laxon et al*., 2013]. Thus, contemporary conditions of snow thickness distribution on Arctic sea ice need to be assessed and reported. This has become particularly important in view of the regime shift of Arctic sea ice to younger thinner ice, which is more susceptible to thermodynamic forcings, emphasizing the greater role of snow thickness in sea ice growth and melt than in earlier decades [*Maykut*, 1986].

Obtaining high-resolution measurements of snow thickness distribution on Arctic sea ice has been challenging. Traditional, in situ observations are limited spatially. More recently, remote-sensing data have become available for the analysis of regional snow thickness. Validation of the accuracy of both airborne and satellite snow depth estimates is required [*Farrell et al*., 2012; *Brucker and Markus*, 2013], and remains the subject in a number of ongoing studies. In this study, we present a new assessment of the spring snow thickness distribution on Arctic sea ice using airborne and in situ measurements at the highest spatial resolution scale currently available. Coordinated in situ snow depth measurements from the Bromine Ozone Mercury Experiment (BROMEX) campaign in March 2012 [*Nghiem et al*., 2013] were used to validate the IceBridge standard and quicklook snow thickness products. The validated snow thickness products were then used to produce an updated climatology of spring snow depth distribution on sea ice in the western Arctic, and quantify the change in snow depth in recent years via comparison with the W99 climatology.

2. Data and Methods

2.1. IceBridge Airborne Data

The Operation IceBridge standard snow depth product was the primary data set used in this study. These data are publicly available on the National Snow and Ice Data Center (NSIDC) website (http://nsidc.org/data/idcsi2) and form part of the "IceBridge Sea Ice Freeboard, Snow Depth, and Thickness Product" [*Kurtz et al*., 2012]. Between 2009 and 2013, Operation IceBridge conducted 45 flights in March and April, before the onset of melt, measuring snow thickness on Arctic sea ice (Figure 1). The snow thickness was measured with the University of Kansas' ultrawideband frequency-modulated continuous wave (FMCW) snow radar using the 2–8 GHz frequency range [*Leuschen*, 2009]. The snow radar pulse-limited footprint is approximately 14.5 m along track and 11 m across track on level sea ice for the nominal flight altitude; the radar echoes are stacked in the snow depth retrieval algorithm to reduce speckle noise, which lessens the along-track resolution to 40 m.

The snow radar has been continually changed and improved, with larger bandwidth and higher signal-to-noise ratio (SNR) [*Panzer et al*., 2013]. The radar bandwidth determines the range resolution, which is 5 cm for 2009–2011 and 4 cm for 2012–2013 [*Panzer et al*., 2013; *Kurtz et al*., 2013]. The snow depth retrieval algorithm was updated to account for changes in the SNR. Subsequently, two algorithms are now used, one to account for the low SNR during the 2009 campaign, and one to adapt to the changing SNR in the 2010 and later campaigns [*Kurtz et al*., 2013]. Due to these continual changes, repeat validation is required to ensure accuracy of the retrieval algorithms. Currently, the uncertainty associated with the IceBridge snow depth

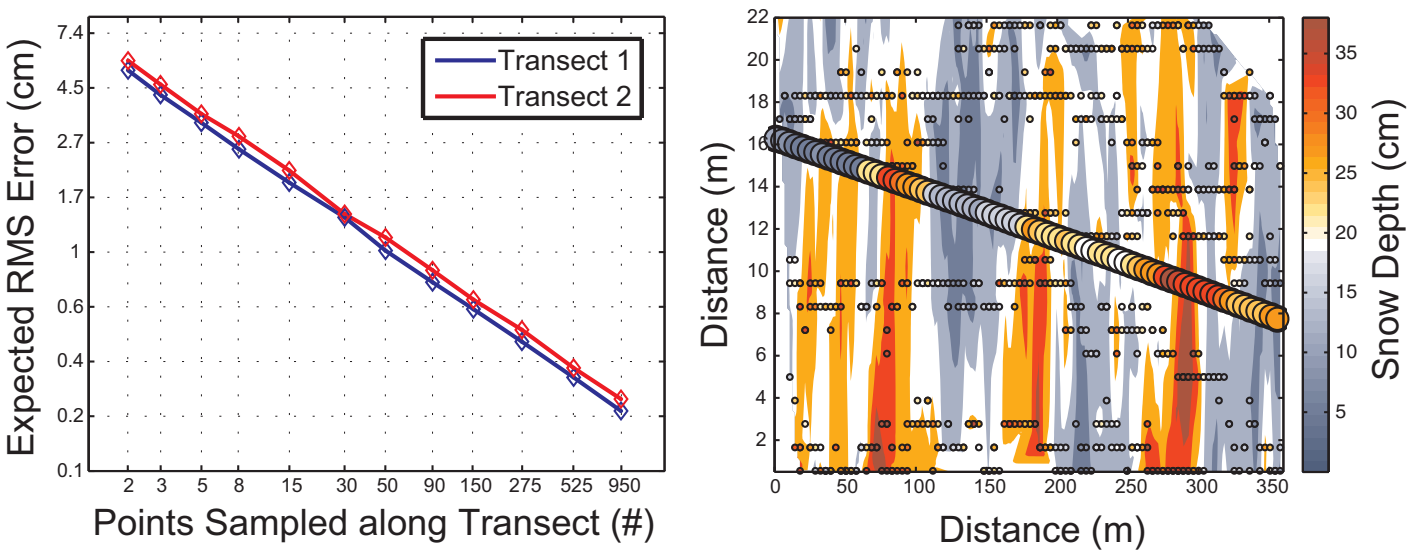

Figure 2. (left) The RMS error of Transects 1 and 2 on Elson Lagoon based on the number of points measured along the transect using a Poisson distribution after *Blanchet and Davidson* [2011] and W99. (right) An interpolation of the in situ data collected along Transect 2. In situ measurements are shown by small circles and the IceBridge quick-look product by bold circles. The color of the circles corresponds to snow depth. Note the differing distance range for the axes.

product is 5.7 cm based on comparisons with in situ data gathered in April 2009 [*Kurtz et al.*, 2013]. The 2013 quick-look data are currently undergoing processing for finalized versions.

Since 2012, IceBridge has provided a quick-look data product within ~1 month of acquisition to facilitate use of the data for seasonal forecasting of the Arctic sea ice cover [*Kurtz et al.*, 2013]. The main differences between the snow radar standard product and quick-look product are the use of lower-quality Global-Positioning-System trajectory data and noise reduction techniques for the field-processed quick-look data. Quantifying the differences in the standard and quick-look data can be done by comparing the two data sets. For the snow depth data, this was done by first gridding the output data from the snow radar to a 25 km polar stereographic grid and examining statistics of the differences. The quick-look data for 2012 were very consistent with the standard data product, with a mean difference as small as 0.05 cm, and standard deviation of differences of 2 cm. There was also no discernible spatial pattern in the differences. For 2013, the mean difference was 1.6 cm and the standard deviation of differences was 2.4 cm. The overall differences were small; however, there was a strong spatial pattern to the differences in multiyear ice areas north of Greenland and Canada, which had several centimeters less snow than the standard data product.

2.2. In Situ Data

Coordinated in situ snow depth measurements were made during the BROMEX field campaign [*Nghiem et al.*, 2013] to validate the IceBridge quick-look and standard snow thickness products. On 15 March 2012, the NASA P-3B aircraft, carrying the Operation IceBridge instrument suite, flew an east-west transect at ~460 m altitude in clear and calm conditions over the BROMEX field site near Barrow, Alaska. These conditions persisted throughout the week as ground-based snow depth measurements were carried out in temperatures ranging from −36.0°C to −30.1°C with wind speeds of 2.7–5.0 m s^{-1} (http://www.esrl.noaa.gov/gmd/dv/). No significant blowing snow events were observed throughout the week of field measurements.

Two ground-truth transects were made underneath the flight path on Elson Lagoon, an area consisting of relatively level, undeformed first year sea ice covered by drifted snow (Figure 2). The standard deviation of the sea ice thickness was less than 15 cm. Snow depths were measured every 1–5 m using a Snow-Hydro© Automated Snow Depth Probe or "MagnaProbe," which has an accuracy of ±0.3 cm on level sea ice and snow. Snow density was measured every ~30 m with a "Federal Sampler" [*Marr*, 1940]. The first transect consisted of three lines approximately 1000 m in length, each 5 m apart, for a width of 10 m. The second transect included five lines roughly 400 m in length, 5 m apart, for a width of 20 m.

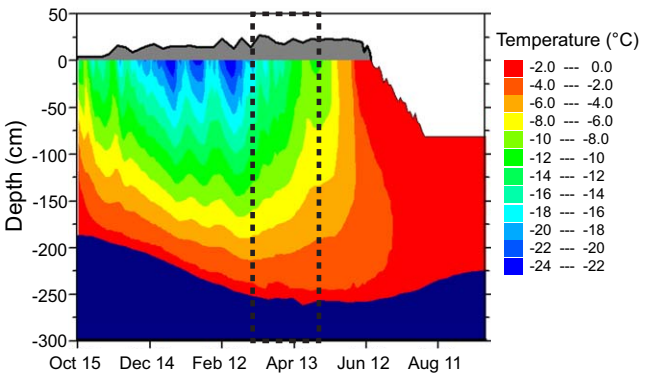

Figure 3. Temperature profiles from an IMB buoy in a multiyear sea ice floe at the Surface Heat Budget of the Arctic Ocean (SHEBA) field campaign. Our analysis focuses on March and April months only, outlined by the black dashed box, which is before the onset of melt.

To estimate the error associated with in situ data, subsets of varying size were randomly selected from the data and averaged. This iterative approach was performed 2000 times. The root-mean-square error was then calculated, providing the expected RMS error of the in situ data according to the number of snow depths measured. This method assumes a Poisson distribution, which has been used in snow depth modeling [*Blanchet and Davidson*, 2011] and in W99. For an average of 16 in situ measurements per snow radar footprint, the expected error was 1.4 cm. The slopes of the first few point measurements in both transects were approximately −0.5, indicating that the 1–5 m spaced measurements were independent of each other (Figure 2). Transects 1 and 2 have similar fitted lines in Figure 2, indicating that both transects were consistently sampled and that the snow depth distributions were not significantly different between the transects.

For the validation analysis, all in situ point measurements within the snow radar footprint were averaged and compared to the IceBridge snow thickness products. No outliers were removed from the in situ or IceBridge data sets. A robust least squares cubic regression line was fitted to the data to account for a varying error in the in situ averages and a constant 5.7 cm uncertainty in the IceBridge products.

The W99 climatology was used for comparison with the contemporary snow depth distribution from the IceBridge products. The analysis focused on March and April months, which we define as our spring study period, because this period offered the most data for comparison (Figure 3). The W99 climatology consists of snow depth data from the Soviet Union's manned drifting ice stations in 1937, 1954–1991. The data are readily available at the NSIDC website [*Fetterer and Radionov*, 2000]. Each "North Pole" station was located on multiyear sea ice, and began its drifting trajectory from the central Arctic Ocean. During its drift, snow depth was measured every 10 m along the same 100 m snowline every ∼10 days throughout the station's lifetime. The snowlines were located on variable surface topography, from level to ridged sea ice. The updated climatology was reproduced following W99.

Snow data from the Cold Regions Research and Engineering Laboratory's (CRREL) Ice Mass Balance (IMB) buoys (D. K. Perovich et al., Observing and understanding climate change: Monitoring the mass balance, motion, and thickness of Arctic sea ice, 2013, http://IMB.crrel.usace.army.mil) were also analyzed and compared to the W99 climatology. The IMB buoys are equipped with acoustic range finders which measure the time between the transmitted signal from the sensor and backscattered signal from the surface, yielding the distance between the buoy sensor and air-snow interface. Using the initial snow and sea ice thicknesses with the measured distances, we extracted information on the change in snow depth during the lifetime of each IMB buoy. The IMB buoys were deployed on both first year and multiyear sea ice mainly in the western and central Arctic in 1993–2013, and new deployments are currently ongoing.

2.3. Snow Depth Interpolation

In order to assess the springtime snow depth distribution from the 2009–2013 IceBridge snow thickness products, we used the same method of W99. A least squares solution was found for the two-dimensional quadratic equation using rectangular coordinates, defined by

$$H = H_o + Ax + By + Cxy + Dx^2 + Ey^2 \quad (1)$$

where H_o is the snow depth at the North Pole, x and y are rectangular coordinates converted from latitudes and longitudes using the Equal-Area Scalable Earth Grid (EASE-Grid) map projection [K. W. Knowles, Points,

pixels, grids, and cells—A mapping and gridding primer, unpublished report, Natl. Snow and Ice Data Cent., Boulder, Colo., 1993], and *A, B, C, D*, and *E* are coefficients. Once the solution was found, snow depth was interpolated between data points, producing a snow depth distribution for a given region based on the data set used.

In W99, gridded averages of Soviet drifting ice station data were used when solving for the least squares solution. We averaged the IceBridge snow thickness product by the same grids for consistency. There are differences between the locations of the Operation IceBridge flights, and the Soviet drifting ice stations. Thus, the analysis was limited to the western Arctic where both data sets overlap. RMS errors were calculated between the interpolated and gridded snow depths for comparison with the errors reported in W99.

The decadal change in spring snow depth was calculated using data from the Soviet drifting ice stations, the IMB buoys, and the IceBridge snow thickness product. These data span 1950–1987, 1993–2013, and 2009–2013, respectively. The anomaly was found by taking each point measurement minus the W99 multiyear average for that location. Each year's spring anomalies were averaged to produce the decadal change between 1950 and 2013.

2.4. Accumulation Rates and Freezeup

The relationships between the reduced snow cover, snow accumulation rates, and sea ice freezeup dates were evaluated using data from the Soviet stations, IMB buoys, and a freezeup product derived from passive microwave satellite data [*Markus et al*., 2009]. Snow accumulation rates were defined as the monthly average snow depth minus the previous month's average snow depth. The sea ice freezeup product covers the entire passive microwave record, 1979–2012, and is currently available on the Cryosphere Research Portal (http://neptune.gsfc.nasa.gov/csb/). For the correlation analysis, we compared the average day of autumn freezeup with the spring snow depth in corresponding areas for both periods.

3. Results and Discussion

3.1. IceBridge Validation

The Figure 2 (right) shows a three-dimensional comparison between the in situ point measurements, represented by small circles, and the IceBridge snow depth product, represented by bold circles. There is good agreement between the two data sets, and also between the IceBridge product and the in situ interpolation. On average, Transect 1 had 26 in situ point measurements within each snow radar footprint, while Transect 2 had 39 point measurements within each snow radar footprint, providing the most densely sampled ground-truth lines for Operation IceBridge to date.

Figure 4 shows the variation between the IceBridge quick-look and standard snow depth products and in situ averages along each transect. Overall, the patterns between the in situ and IceBridge data sets agree well, and the differences between their averages are within the estimated uncertainties. The RMS error between the IceBridge quick-look product and the in situ averages was 5.8 cm, comparable to the estimated uncertainty of 5.7 cm for the 2009–2011 IceBridge snow depth products [*Kurtz et al*., 2012].

However, the IceBridge product appears to underestimate thin snow depths in comparison to the in situ averages, and a clear discrepancy can be seen around 50 m along Transect 2 (Figure 4); this discrepancy is also apparent in the scatter plot (Figure 5) where the IceBridge quick-look and standard products estimate a snow thickness of ∼5–8 cm while the in situ mean is ∼23 cm. It is unclear why this low bias exists. The value of snow density used in the IceBridge retrieval algorithm is 320 kg m^{-3}, while the measured snow density along the two transects was 332 $\pm$ 13 kg m^{-3}. This density difference leads to a ∼0.1 cm snow depth difference, which is not enough to explain the bias nor why the bias is most prominent at low snow values. An examination of the radar echogram in the low areas shows the chosen snow-ice interface was smooth and consistent over this region, but the backscatter was low compared to the surrounding ice (Figure 6). At a distance of 350–400 m along Transect 2, the high IceBridge snow depth estimates are likely due to the presence of coherent noise in the radar data.

In short, the above data demonstrate that the IceBridge snow depth product can accurately measure snow depth on level, undeformed sea ice, but the anomalies also underscore the need for more validation efforts to fully resolve the sources of error in snow depth estimates over different sea ice types and roughness

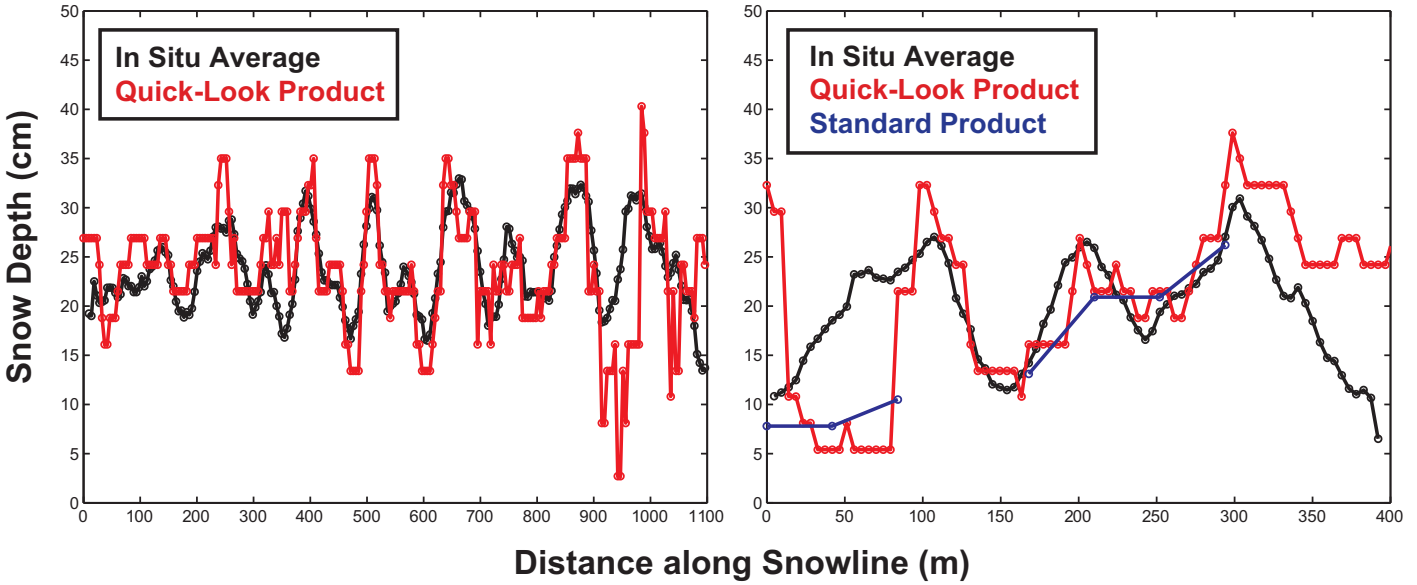

Figure 4. Comparisons between the in situ averages (black), the IceBridge quick-look snow depth product (red), and, where available, the IceBridge standard product (blue) along Transects (left) 1 and (right) 2. Transects 1 and 2 were ~1000 and ~400 m in length, respectively.

conditions. Considering the good agreement between the IceBridge products and in situ data, we use a one-to-one relationship for estimating snow depth distributions in the western Arctic.

3.2. Climatology

The spring snow depth distributions estimated from the IceBridge and the Soviet station data sets using equation (1) are shown in Figure 7, along with their point measurements. There is a marked decrease in snow thickness spanning the western Arctic in 2009–2013 compared to the 1937, 1954–1991 climatology. An average snow depth of 35.1 ± 9.4 cm was observed in the W99 climatology for the western Arctic; the 2009–2013 average was 22.2 ± 1.9 cm, suggesting a thinning of 37 ± 29% (Figure 7). The Beaufort and Chukchi seas exhibited the greatest change, having thinned by approximately 56 ± 33% (Figure 8). The RMS error between the 2009–2013 in situ and interpolated snow depths was 1.9 cm, and significantly lower than the reported error of 9.4 cm in the W99 climatology. The decadal change in spring snow depth revealed a trend of −0.29 cm/yr with 99% significance (Figure 9). In comparison, the largest trend found by W99 was approximately −0.10 cm/yr for May, the month of maximum snow depth, in 1950–1991.

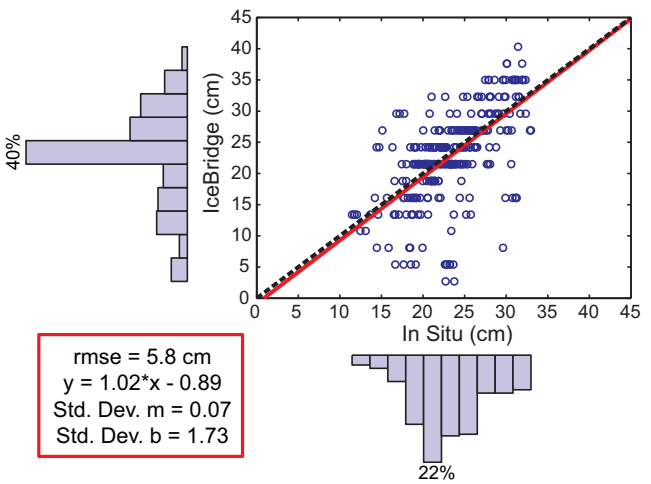

Figure 5. The least squares cubic regression (red line) between the IceBridge quick-look data (*y* axis) and the in situ averages (*x* axis). The one-to-one line is shown by the black dashed line. Both histograms have 10 bins, and the values of the largest bins are a percentage of the normalized distributions.

According to *Kurtz and Farrell* [2011], IceBridge snow depth measurements for 2009 were 52% thinner in areas of first year sea ice than the 1937, 1954–1991 climatology. Our findings also show thinner snow depths in the Beaufort and Chukchi seas, where much of the sea ice is younger [*Richter-Menge and Farrell*, 2013] and later sea ice freezeup dates have been observed [*Markus et al.*, 2009]. A

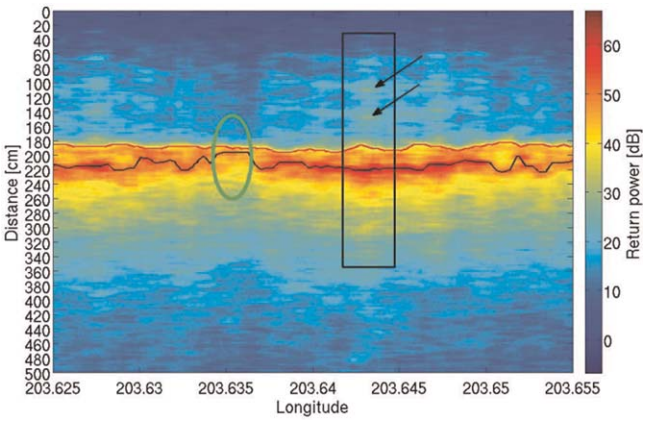

Figure 6. The radar echogram of Transect 2. The red line is the chosen snow-air interface and the chosen black line is the chosen snow-ice interface. The area with the green circle shows the ~0–100 m region of Transect 2 where thin snow depths were identified. The black box area shows where thick snow depths were chosen, and the arrows point to the presence of coherent noise in the radar data.

modeling study by *Hezel et al*. [2012] projected snow depths on Arctic sea ice using the first-order effects of sea ice freezeup dates and precipitation rates. There was good agreement between the IceBridge and modeled snow depth distributions in the western Arctic, both in space and magnitude. The 2009–2013 IceBridge average was 22.2 ± 1.9 cm, while the modeled 1981–2000 and 2081–2100 averages were 28 ± 7 cm and 16 ± 5 cm, respectively [*Hezel et al*., 2012].

3.3. Accumulation Rates and Freezeup

While there are numerous processes that affect spring snow thickness on Arctic sea ice, snow accumulation rates and the timing of sea ice freezeup directly affect spring snow thickness the most; they are considered to have first-order effects on snow depth [*Radionov et al*., 1997; *Hezel et al*., 2012]. The comparison between the CRREL IMB buoy and the Soviet ice station data showed no significant changes in monthly snow accumulation rates, with the exception of April (Figure 10). In April, the Soviet station and IMB buoy data yielded accumulation rates of 3.3 ± 1.1 and 0.6 ± 0.4 cm/month, respectively. The differences in accumulation rates for all other months were smaller than their standard errors (Figure 10). Note that the large standard errors in the IMB buoy data are due to the sample size rather than the quality of the buoy data; there were 8–17 IMB buoys per month for 2009–2013. The maximum snow accumulation rates for the Soviet station and IMB buoy data occurred in September, and were 6.5 ± 1.7 and 7.5 ± 2.0 cm/month, respectively. The differences in snow accumulation rates, particularly the maximum rates, were not large enough to explain the observed decrease in snow depths across the western Arctic. In addition, the annual snow accumulations from the Soviet drifting ice stations and the IMB buoys were comparable with values of 30.1 ± 3.2 and 28.5 ± 3.9 cm, respectively (Figure 10). These results were also consistent with multiple reanalysis products showing no trend in the 1981–2010 annual precipitation for our region of study [*Lindsay et al*., 2014].

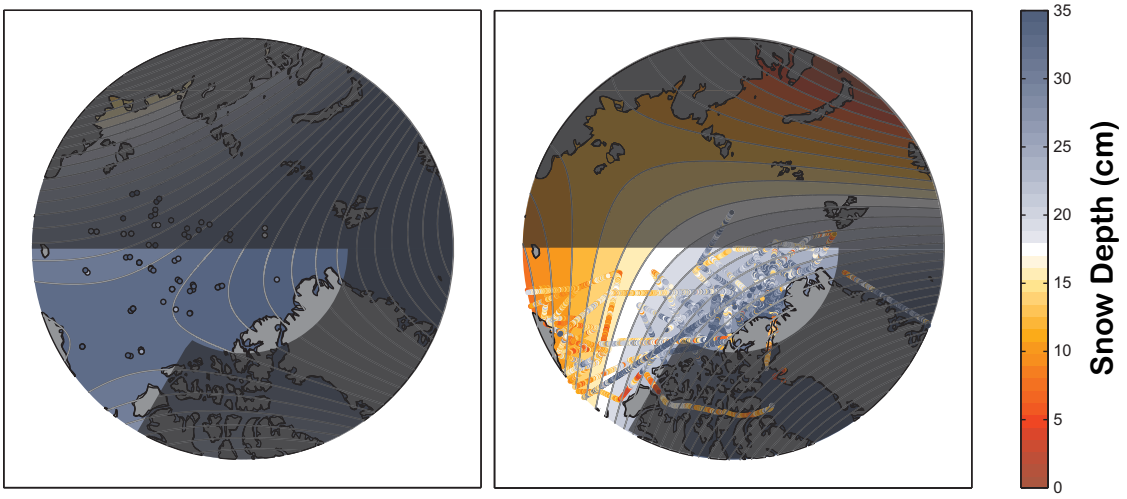

Figure 7. The snow depth distribution resulting from the two-dimensional quadratic equation (equation (1)) fitted to the 1937, 1954–1991 (left) Soviet drifting ice station data and (right) the 2009–2013 IceBridge snow depth products for March and April. Point measurements are indicated by the small circles; snow depths are indicated by color. The gray shading indicates areas where no data are available.

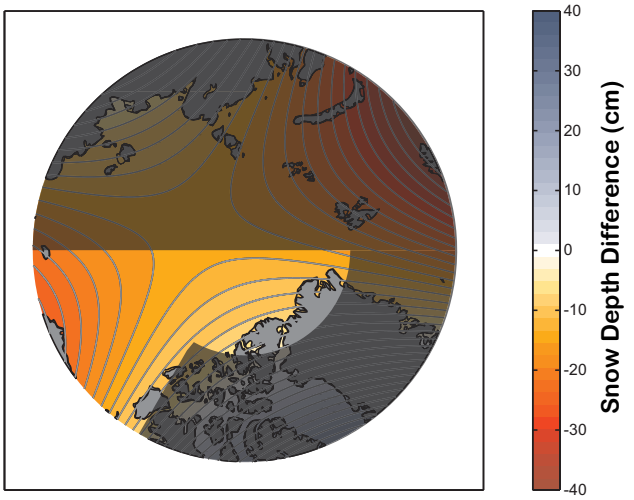

Figure 8. The difference between the 2009–2013 IceBridge snow depth distribution and the W99 climatology. Red indicates that the snow cover has thinned compared to the W99 snow climatology, white indicates no change in snow depths, and blue represents an increase. The gray shading indicates areas where no data are available.

Because maximum snow accumulation rates occur in September and sea ice freezeup is now trending later in autumn in this region [*Markus et al.*, 2009], snow falls directly into the ocean until sea ice forms, resulting in a thinner, cumulative snow cover. The results of sea ice freezeup dates and snow thickness distributions for the 2009–2013 and 1937, 1954–1991 periods are shown in Figure 11. The upper plots represent the 2009–2013 period with sea ice freezeup in the left and snow depth distribution in the right. We found a good spatial match between sea ice freezeup and snow thickness distribution, with a correlation coefficient of −0.68. The strong correlation indicates that the delay in sea ice freezeup may significantly contribute to the decrease in snow depth. Because the correlation coefficient is not exactly −1.0, it also indicates that other factors play a role, such as changes in atmospheric patterns, sea ice motion and deformation, and snow redistribution. The Beaufort and Chukchi seas exhibit later sea ice freezeup and thinner snow depths, which is consistent with the shift to younger sea ice types in this region [*Nghiem et al.*, 2007; *Maslanik et al.*, 2011]. The Lincoln Sea, being mostly composed of multiyear sea ice, has the earliest freezeup and the thickest snow depths. The lower plots show the 1937, 1954–1991 period of sea ice freezeup and snow thickness distribution. The sea ice freezeup and snow thickness distribution had a correlation coefficient of −0.23 for the 1979–1991 period. Note that sea ice freezeup for this period was calculated based on the available satellite passive microwave record from 1979–1991, and the lack of data prior to 1979 might possibly contribute to the low correlation.

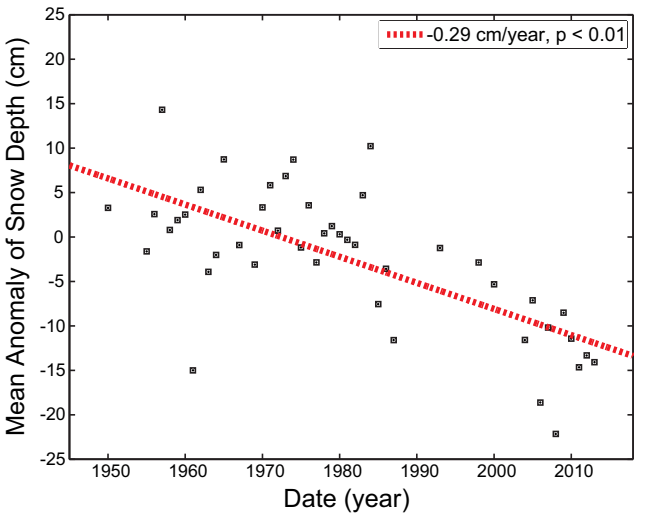

Figure 9. The decadal change in snow depth in spring. The anomalies were calculated using data from Soviet drifting ice stations (1950–1987), Ice Mass Balance buoys (1993–2013), and the Operation IceBridge snow depth products (2009–2013). The anomaly is the measurement minus the W99 multiyear average in spring at that location. The average of the anomalies for each year is shown by black squares, and the red line represents the trend in centimeters per year. For measurements within the western Arctic only, the trend was −0.27 cm/yr with 99% significance.

While earlier melt onset has substantial effects on the surface albedo and progression of melt in late spring and early summer, it does not impact the spring snow thickness as much as the timing of sea ice freezeup. The melt onset occurs in June for the western Arctic and late May for the Beaufort and Chukchi seas in 2009–2013 [*Markus et al.*, 2009]. If we subtract the May accumulations (Figure 10) due to melt from the total accumulation, and separately, subtract September accumulations due to later freezeup from the total, the loss of snow in September is larger than the loss in May, indicating that September snow loss due to delayed freezeup has a greater impact on the cumulative snow accumulation than the snow loss in May due to earlier melt onset.

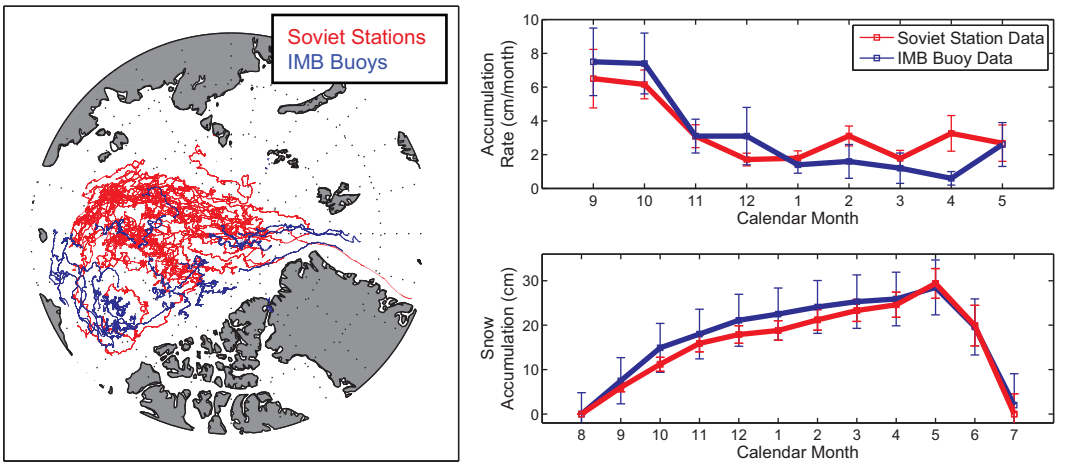

Figure 10. (left) The locations of the CRREL Ice Mass Balance buoys (blue) and Soviet drifting ice stations (red). (top right) The average monthly snow accumulation rate according to Ice Mass Balance buoy data (blue) and the Soviet drifting ice stations snowline data (red). Rates and their standard errors are given in centimeters per month (*y* axis), and the months are given by calendar number beginning with September (*x* axis). (bottom right) Snow accumulation as a function of time, with Soviet station data in red and IMB buoy data in blue.

Our study focuses on the March and April period, which is before the onset of melt in this region for both periods [*Markus et al.*, 2009].

Using the freezeup product and IMB and W99 accumulation rates, we found that later freezeup dates may explain the magnitude of decrease in snow depth shown in Figures 8 and 9. On average for the 2008–2012 period, the continual freezeup occurred on September 18 for the western Arctic, and October 22 for the Beaufort and Chukchi seas. Taking the monthly snow accumulation (Figure 10), dividing it by the number of

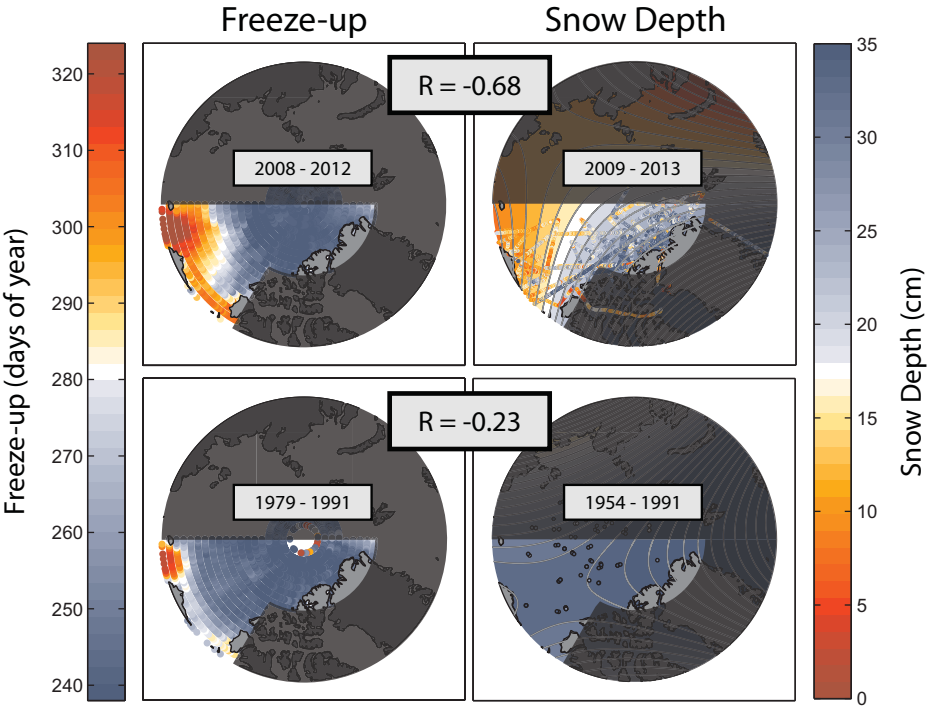

Figure 11. The correlations between (left) sea ice freezeup dates and (right) snow depth distributions for the 2009–2013 and 1954–1991 periods. Later freezeup dates are represented by red shading while earlier freezeup dates are represented by blue shading. Note that freezeup dates are given in Days of Year, and ranges from approximately late August to late November. (top left) Sea ice freezeup dates for the 2008–2012 period. (top right) Snow depth distribution according for the 2009–2013 period. (bottom left) Sea ice freezeup dates for the 1979–1991 period. (bottom right) The W99 snow depth climatology.

Table 1. Mid-December Estimates[a]

	Young Ice (2009–2013)	Young Ice (1954–1991)	First Year Ice (1954–1991)	Multiyear Ice (1954–1991)
Ice thickness (m)	0.75	1.2	1.4	3
[Reference]	[*Zhang and Rothrock*, 2003]	[*Thorndike et al.*, 1975]	[*Kwok and Cunningham*, 2008]	[*Kwok and Cunningham*, 2008]
Snow density (kg m^{-3})	290	300	300	300
[Reference]	[*Kwok and Cunningham*, 2008]	[W99; *Kwok and Cunningham*, 2008]	[W99]	[W99]
December snow depth (m)	0.088 ± 0.029	0.287 ± 0.094	0.287 ± 0.094	0.287 ± 0.094
Surface heat flux (W m^{-2})	79–85	43–49	39–43	20–22

[a]Ice thicknesses, snow densities, December snow depths, and the resulting surface heat fluxes for varying ice types in mid-December conditions assuming an air temperature of −34°C and under ice temperature of −1.8°C [*Maykut and Untersteiner*, 1971; *Maykut*, 1978].

days pertaining to the month, we get an accumulation per day for the corresponding month. The delay in sea ice freezeup results in a 4.5 ± 1.2 cm total loss in the western Arctic, and a 12.8 ± 2.4 cm total loss in the Beaufort and Chukchi seas. These results are consistent with and within the errors of the differences between the W99 and IceBridge results: 12.9 ± 9.6 cm for the western Arctic, and 18.3 ± 9.6 cm for the Beaufort and Chukchi seas. When taking into account that snow accumulation is greatest during the early autumn, the delay in freezeup appears to have a significant impact on spring snow thickness on sea ice in the western Arctic.

We assessed the significance of a thinner snow cover on winter surface heat fluxes for a variety of ice types representative of the W99 and 2009–2013 periods and assumed mid-December conditions for sea ice thicknesses, air temperature, under-ice temperature, and snow densities in the Beaufort and Chukchi seas (Table 1). Based on the IceBridge snow thickness distribution for 2009–2013, the Beaufort and Chukchi seas have an average snow depth of 14.5 cm in spring. A mid-December snow depth can be estimated by subtracting the cumulative snow accumulation based on the monthly snow accumulation rates. Using the IMB buoy accumulation rates, the total snow accumulation between mid-December and the end of March was 5.8 ± 2.2 cm, yielding a mid-December snow depth of 8.8 ± 2.9 cm in the Beaufort and Chukchi seas.

To find the surface heat flux, the thermal heat conductance of the sea ice and snow cover was calculated first. The thermal heat conductance was determined using

$$\gamma = k_i k_s / (k_s H + k_i h) \tag{2}$$

where γ is the thermal heat conductance (W m^{-2} °C^{-1}), k_i is the conductivity of the top of the sea ice and a constant of 2.14 W m^{-2} °C^{-1} [*Maykut*, 1978; *Pringle et al.*, 2006], and k_s is the conductivity of the snow, estimated as a function of snow density following *Sturm et al.* [1997]. The surface heat flux was then calculated as a function of the thermal heat conductance and the vertical temperature gradient as shown in

$$F_c = \gamma (T_b - T_0) \tag{3}$$

where F_c is the surface heat flux, γ is the thermal heat conductance found in equation (2), T_b is the temperature at the bottom of the sea ice, and T_0 is the temperature at the surface of the snow. The resulting surface heat flux through 0.75 m thick sea ice and 8.8 ± 2.2 cm thick snow cover was ∼79–85 W m^{-2}. Applying the W99 snow climatology and accumulation rates, the W99 mid-December mean snow depth was 28.7 ± 9.4 cm, yielding a surface heat flux of ∼43–49 W m^{-2} on young ice, ∼39–43 W m^{-2} on first year ice, and ∼20–22 W m^{-2} on multiyear ice (Table 1).

The timespan between initial snow accumulation after sea ice freezeup and mid-December is smaller in the 2009–2013 period compared to the 1954–1991 period, leaving less time for snow to densify. To explore the impact of lower bulk snow densities on surface heat fluxes, we performed a sensitivity study of snow density. Typically, snow density increases the fastest during the autumn when storms generate large snowfalls and wind packing occurs [*Radionov et al.*, 1997; W99; *Sturm et al.*, 2002]. Bulk snow densities in the sensitivity study ranged from 200 kg m^{-3}, representing new and recent snow, to 300 kg m^{-3}, representing typical December wind-packed snow [*Sturm et al.*, 2002]. Densities greater than 300 kg m^{-3} were excluded since observations have shown that snow density remains relatively constant until the onset of spring melt. [W99; *Kwok and Cunningham*, 2008]. In the sensitivity analysis, the maximum difference in surface heat flux was ∼1 W m^{-2} for all ice types when using a snow density of 200 kg m^{-3} instead of 300 kg m^{-3}. Otherwise, the changes in surface heat flux due to smaller differences in snow densities were negligible.

4. Conclusions

This study has shown that the airborne radar used on Operation IceBridge can accurately measure snow depth on level, first year sea ice. This finding of "local" accuracy is enough to warrant the use of the extensive IceBridge snow depth data to assess snow cover trends across the Arctic Basin. Ongoing and future validation efforts on more complex sea ice topography will allow us to improve our accuracy when using the data, and for now, these data provide the highest spatial resolution of spring snow thickness. For the 2009–2013 period, the products show that snow has decreased by 37 $\pm$ 29% in the western Arctic and by 56 $\pm$ 33% in the Beaufort and Chukchi seas, compared to the 1954–1991 snow depth climatology produced by W99. These are large changes in snow depth distributions, and the implications are significant for future sea ice in the region. The changes could arise from changes in winter precipitation, changes in the date when the ice will hold snow, or a combination of both.

Addressing the latter point, we provided evidence showing that monthly and annual snow accumulations have not changed in magnitude or timing using IMB buoy and W99 data. The results imply that either snowfall rates and snow redistribution have not changed, or the combined effect of their changes has canceled any potential snow accumulation loss. We found a strong correlation between the timing of sea ice freezeup and the reduction in spring snow thickness, which is consistent with the shift to first year and young sea ice types in this region [*Nghiem et al.*, 2007; *Maslanik et al.*, 2011] and with snow depth measurements on younger ice types [*Radionov et al.*, 1997]. In future scenarios, delayed sea ice freezeup and increasing winter precipitation are expected, which underscores the need for continual monitoring of the snow cover on Arctic sea ice.

The combined effect of reduced snow cover and young ice based on the 2009–2013 results yielded surface heat fluxes nearly double than that on young ice in the 1954–1991 period, and nearly quadruple than that on multiyear sea ice, regardless of differences in snow density. These results have several implications for the sea ice climate system. They indicate that: (1) the current and projected shift to younger ice types and a thinner snow cover in the Arctic will result in larger net outgoing longwave radiation during the autumn and winter seasons than in the 1954–1991 period, (2) the increase in heat input to the atmospheric boundary layer will likely increase the atmospheric moisture content, affecting precipitation rates, and (3) with a delayed, thinner sea ice cover, snowfall rates, regardless of change, will have an increasingly important role in the surface heat exchange during the autumn and winter seasons.

While the observed change in snow thickness distribution is consistent with the first-order effects of unchanged snow accumulation rates and delayed sea ice freezeup, there are local processes that should be considered when interpreting our results. Sea ice motion and deformation, blowing snow, changes in snow redistribution and sea ice roughness, increased precipitation due to more open water areas, and altered atmospheric patterns, all likely contribute to changes in the snow depth distribution. Of particular interest is the shift to younger ice types, and the effects of their reduced surface roughness on drifting snow. The exact contributions of such processes are largely unknown due to the scarcity of collocated and contemporaneous datasets. These processes may be investigated in future validation efforts with better spatial resolution and more frequent coverage of airborne and satellite measurements, as well as with modeling studies that continue to develop and improve complex feedbacks. Impacts of these local processes may be better understood through the synthesis of future observational, modeling, and remote sensing work, especially with the advent of ICESat2 in 2017.

Acknowledgments
Snow data from the 2012 BROMEX field campaign are available upon request. Meteorological data are available at http://www.esrl.noaa.gov/gmd/dv/. The IceBridge quick-look and standard snow depth products are available at https://nsidc.org/data/docs/daac/icebridge/evaluation_products/sea-ice-freeboard-snowdepth-thickness-quicklook-index.html and http://nsidc.org/data/idcsi2.html. The Soviet station snow data are available at http://dx.doi.org/10.7265/N5MS3QNJ. Ice Mass Balance buoy data are available at http://IMB.crrel.usace.army.mil. The sea ice freezeup product from passive microwave satellite data is available at http://neptune.gsfc.nasa.gov/csb/index.php?section=54. This research was supported by the National Aeronautics and Space Administration (NASA), and by contributors to the U.S. Interagency Arctic Buoy Program, which include the U.S. Coast Guard, NAVO, NIC, NOAA, NSF, and ONR. This is JISAO contribution 2225. The research carried out at the Jet Propulsion Laboratory, California Institute of Technology, was supported by the NASA Cryospheric Sciences Program. We thank Jacqueline A. Richter-Menge of the U.S. Army Cold Regions Research and Engineering Laboratory for the planning and coordination of the IceBridge flight operation with the BROMEX field campaign, and Stephen Warren for helpful discussions. We thank UMIAQ, the Barrow whaling community, and the Barrow Arctic Science Consortium for their assistance in the BROMEX field campaign.

References

Arrigo, K. R., G. Dijken, and S. Pabi (2008), Impact of a shrinking Arctic ice cover on marine primary production, *Geophys. Res. Lett.*, *35*, L19603, doi:10.1029/2008GL035028.

Blanchet, J., and A. C. Davidson (2011), Spatial modeling of extreme snow depth, *Ann. Appl. Stat.*, *5*(3), 1699–1725, doi:10.1214/11-AOAS464.

Blazey, B. A., M. M. Holland, and E. C. Hunke (2013), Arctic Ocean sea ice snow depth evaluation and bias sensitivity in CCSM, *Cryosphere Discuss.*, *7*, 1495–1532, doi:10.5194/tcd-7–1495-2013.

Brucker, L., and T. Markus (2013), Arctic-scale assessment of satellite passive microwave-derived snow depth on sea ice using Operation IceBridge airborne data, *J. Geophys. Res. Oceans*, *118*, 2892–2905, doi:10.1002/jgrc.20228.

Eicken, H., T. C. Grenfell, D. K. Perovich, J. A. Richter-Menge, and K. Frey (2004), Hydraulic controls of summer Arctic pack ice albedo, *J. Geophys. Res.*, *109*, C08007, doi:10.1029/2003JC001989.

Farrell, S. L., N. T. Kurtz, L. Connor, B. Elder, C. Leuschen, T. Markus, D. C. McAdoo, B. Panzer, J. Richter-Menge, and J. Sonntag (2012), A first assessment of IceBridge snow and ice thickness data over Arctic sea ice, *IEEE Trans. Geosci. Remote Sens.*, *50*(6), 2098–2111, doi:10.1109/TGRS.2011.2170843.

Fetterer, F., and V. Radionov (2000), *Arctic Climatology Project. Environmental Working Group Arctic Meteorology and Climate Atlas* [CD-ROM], Natl. Snow and Ice Data Cent., Boulder, Colo., doi:10.7265/N5MS3QNJ.
Grebmeier, J. M., S. E. Moore, J. E. Overland, K. E. Frey, and R. Gradinger (2010), Biological response to recent Pacific Arctic sea ice retreats, *Eos Trans. AGU*, *91*(18), 161–168.
Hezel, P. J., X. Zhang, C. M. Bitz, B. P. Kelly, and F. Massonnet (2012), Projected decline in spring snow depth on Arctic sea ice caused by progressively later autumn open ocean freeze-up this century, *Geophys. Res. Lett.*, *39*, L17505, doi:10.1029/2012GL052794.
IPCC (2013), *Climate Change 2013: The Physical Science Basis. Contribution of Working Group I to the Fifth Assessment Report of the Intergovernmental Panel on Climate Change*, edited by T. F. Stocker et al., 1535 pp., Cambridge Univ. Press, Cambridge, U. K.
Kurtz, N., and S. Farrell (2011), Large-scale surveys of snow depth on Arctic sea ice from Operation IceBridge, *Geophys. Res. Lett.*, *38*, L20505, doi:10.1029/2011GL049216.
Kurtz, N., M. Studinger, J. Harbeck, V. D. Onana, and S. Farrell (2012), *IceBridge Sea Ice Freeboard, Snow Depth, and Thickness*, Version 1, NASA DAAC at the Natl. Snow and Ice Data Cent., Boulder, Colo.
Kurtz, N., S. L. Farrell, N. Galin, J. P. Harbeck, R. Lindsay, V. D. Onana, B. Panzer, and J. G. Sonntag (2013), Sea ice thickness, freeboard, and snow depth products from Operation IceBridge airborne data, *Cryosphere*, *7*, 1035–1056, doi:10.5194/tc-7–1035-2013.
Kwok, R., and G. F. Cunningham (2008), ICESat over Arctic sea ice: Estimation of snow depth and ice thickness, *J. Geophys. Res.*, *113*, C08010, doi:10.1029/2008JC00475.
Kwok, R., and D. A. Rothrock (2009), Decline in Arctic sea ice thickness from submarine and ICESat records: 1958–2008, *Geophys. Res. Lett.*, *36*, L15501, doi:10.1029/2009GL039035.
Laxon S., et al. (2013), CryoSat-2 estimates of Arctic sea ice thickness and volume, *Geophys. Res. Lett.*, *40*, 732–737, doi:10/1002/grl.50193.
Leuschen, C. (2009), *IceBridge Snow Radar L1B Geolocated Radar Echo Strength Profiles*, Natl. Snow and Ice Cent., Boulder, Colo. [Updated this year.]
Lindsay, R., M. Wensnahan, A. Schweiger, and J. Zhang (2014), Evaluation of seven different atmospheric reanalysis products in the Arctic, *J. Clim.*, *27*, 2588–2606, doi:10.1175/JCLI-D-13–00014.1.
Markus, T., J. C. Stroeve, and J. Miller (2009), Recent changes in Arctic sea ice melt onset, freezeup, and melt season length, *J. Geophys. Res.*, *114*, C12024, doi:10.1029/2009JC005436.
Marr, J. C. (1940), *Snow Surveying*, pp. 9–11, U.S. Dept. of Agric., Technol. and Eng., Univ. of Vir., Charlottesville, Va.
Maslanik, J., J. Stroeve, C. Fowler, and W. Emery (2011), Distribution and trends in Arctic sea ice age through spring 2011, *Geophys. Res. Lett.*, *38*, L13502, doi:10.1029/2011GL047735.
Maykut, G. A. (1978), Energy exchange over young sea ice in the central Arctic, *J. Geophys. Res.*, *83*, 8C0241, doi:10.1029/JC083iC07p03646.
Maykut, G. A. (1986), The surface heat and mass balance, in *The Geophysics of Sea Ice*, edited by N. Untersteiner, pp. 395–465, Plenum, N. Y.
Maykut, G. A., and N. Untersteiner (1971), Some results from a time-dependent thermodynamic model of sea ice, *J. Geophys. Res.*, *76*(6), 1550–1575, doi:10.1029/JC076i006p01550.
National Academies (2012), *Seasonal to Decadal Predictions of Arctic Sea Ice—Challenges and Strategies, Polar Research Board, National Research Council*, 92 pp., Natl. Acad. Press, Washington, D. C.
Nghiem, S. V., I. G. Rigor, D. K. Perovich, P. Celemente-Colon, J. W. Weatherly, and G. Neumann (2007), Rapid reduction of Arctic perennial sea ice, *Geophys. Res. Lett.*, *34*, L19504, doi:10.1029/2007GL031138.
Nghiem, S. V., et al. (2013), Studying bromine, ozone, and mercury in the Arctic, *Eos Trans. AGU*, *94*(33), 289–291.
Overpeck, J. T., et al. (2005), Arctic system on trajectory to new, seasonally ice-free state, *Eos Trans. AGU*, *86*(34), 209–316.
Panzer, B., D. Gomez-Garcia, C. Leuschen, J. Paden, F. Rodriguez-Morales, A. Patel, T. Markus, B. Holt, and P. Gogineni (2013), An ultra-wideband, microwave radar for measuring snow thickness on sea ice and mapping near-surface internal layers in polar firn, *J. Glaciol.*, *59*(214), 244–254, doi:10.3189/2013JoG12J128.
Perovich, D. K., and C. Polashenski (2012), Albedo evolution of seasonal Arctic sea ice, *Geophys. Res. Lett.*, *39*, L08501, doi:10.1029/2012GL051432.
Perovich, D. K., B. Light, H. Eicken, K. F. Jones, K. Runciman, and S. V. Nghiem (2007), Increasing solar heating of the Arctic Ocean and adjacent seas, 1979–2005: Attribution and role in the ice-albedo feedback, *Geophys. Res. Lett.*, *34*, L19505, doi:10.1029/2007GL031480.
Perovich, D. K., T. C. Grenfell, B. Light, and P. V. Hobbs (2002), Seasonal evolution of the albedo of multiyear Arctic sea ice, *J. Geophys. Res.*, *107*(C10), 8044, doi:10.1029/2000JC000438.
Petrich, C., H. Eicken, C. M. Polashenski, M. Sturm, J. P. Harbeck, D. K. Perovich, and D. C. Finnegan (2012), Snow dunes: A controlling factor of melt pond distribution on Arctic sea ice, *J. Geophys. Res.*, *117*, C09029, doi:10.1029/2012JC008192.
Pringle, D. J., H. J. Trodahl, and T. G. Haskell (2006), Direct measurement of sea ice thermal conductivity: No surface reduction, *J. Geophys. Res.*, *111*, C05020, doi:10.1029/2005JC002990.
Radionov, V. F., N. N. Bryazgin, and E. I. Alexandrov (1997), The Snow cover of the Arctic Basin, *Tech. Rep. APL-UW-TR 9701*, 95 pp., Appl. Phys. Lab., Univ. of Wash., Seattle, Wash.
Richter-Menge, J. A., and S. L. Farrell (2013), Arctic sea ice conditions in spring 2009–2013 prior to melt, *Geophys. Res. Lett.*, *40*, 5888–5893, doi:10.1002/2013GL058011
Stroeve, J. C., M. C. Serreze, M. M. Holland, J. E. Kay, J. Malanik, and A. P. Barrett (2012), The Arctic's rapidly shrinking sea ice cover: A research synthesis, *Clim. Change*, *110*, 1005–1027, doi:10.1007/s10584-011-0101-1.
Sturm, M., J. Holmgren, M. König, and K. Morris (1997), The thermal conductivity of seasonal snow, *J. Glaciol.*, *43*, 26–41.
Sturm, M., D. K. Perovich, and J. Holmgren (2002), Thermal conductivity and heat transfer through the snow on the ice of the Beaufort Sea, *J. Geophys. Res.*, *107*(C21), 8043, doi:10.1029/2000JC000409.
Thorndike, A. S., D. A. Rothrock, G. A. Maykut, and R. Colony (1975), The thickness distribution of sea ice, *J. Geophys. Res.*, *80*(33), 4501–4513.
Warren, S., I. Rigor, N. Untersteiner, V. F. Radionov, N. N. Bryazgin, Y. I. Aleksandrov, and R. Colony (1999), Snow depth on Arctic sea ice, *J. Clim.*, *12*, 1814–1829.
Wassmann, P., C. M. Duarte, S. Agusti, and M. K. Sejr (2011), Footprints of climate change in the Arctic marine ecosystem, *Global Change Biol.*, *17*, 1235–1249.
Zhang, J, and D. A. Rothrock (2003), Modeling global sea ice with a thickness and enthalpy distribution model in generalized curvilinear coordinates, *Mon. Wea. Rev.*, *131*, 681–697.